J Solid State Electrochem (2002) 6: 225–230
DOI 10.1007/s100080100238

ORIGINAL PAPER

Guor-Bin Jung · Ta-Jen Huang · Chung-Liang Chang

Effect of temperature and dopant concentration on the conductivity of samaria-doped ceria electrolyte

Received: 8 February 2001 / Accepted: 30 May 2001 / Published online: 13 October 2001

Abstract The conductivity, σ, of a samaria-doped ceria electrolyte is studied as a function of temperature and dopant concentration, x, which was from 5 to 30 mol%. It is shown that a maximum in σ versus x corresponds to a minimum in activation energy. It is found that the conductivity is completely due to oxygen vacancy conduction. The conductivity increases with increasing samaria doping and reaches a maximum for $(CeO_2)_{0.8}(SmO_{1.5})_{0.2}$, which has a conductivity of 5.6×10^{-1} S/cm at 800 °C. A curvature at $T = T_c$, the critical temperature, has been observed in the Arrhenius plot. This phenomenon may be explained by a model which proposed that, below T_c, nucleation of mobile oxygen vacancies into ordered clusters occurs, and, above T_c, all oxygen vacancies appear to be mobile without interaction with dopant cation. In addition, the composition dependences of both the critical temperature and the trapping energy are consistent with that of the activation energy.

Keywords Conductivity · Oxygen vacancy · Critical temperature · Samaria-doped ceria

Symbols A: preexponential term in the Arrhenius equation · C: density of equivalent sites · d: pellet thickness · D: diffusion coefficient · E_a: activation energy · f: geometrical factor · ΔG_m: motional free energy ΔG_t: Gibbs free energy for trapping liquid vacancies into clusters · ΔH_t: trapping energy between vacancies and cations · k: Boltzman constant · l: distance to the nearest-neighbor equivalent site · n_c: fraction of the equivalent sites which are empty · n_c*: total fraction of oxygen vacancies · q: charge · R: resistivity of the pellet · T: temperature · x: dopant concentration, mole fraction · z: number of nearest-neighbor equivalent sites · σ: conductivity · v_o: optical-mode attempt frequency for a jump · μ: oxygen vacancy mobility

G.-B. Jung · T.-J. Huang (✉)
Department of Chemical Engineering,
National Tsing Hua University, Hsinchu,
Taiwan 300, Republic of China
E-mail: tjhnang@che.nthu.edu.tw

C.-L. Chang
Industrial Technology Research Institute,
Hsinchu, Taiwan 300, Republic of China

Introduction

Oxides of the fluorite structure, when doped with divalent and trivalent cations, form good solid electrolytes at elevated temperature [1, 2]. In these electrolytes the current is carried by oxygen vacancies that are introduced to compensate for the lower charge of the dopant cations.

Doped zirconia has been most widely used in various applications, such as oxygen sensors and high-temperature fuel cells [3, 4], but it has been shown that ceria has an important advantage over zirconia: ceria achieves higher conductivity than zirconia for the same dopant concentration [5]. In other words, it promises a lowering of the operating temperature from 1000 to 800 °C, which would allow greater flexibility in the choice of electrodes and interconnectors, among other advantages. The disadvantage of a ceria electrolyte is the tendency to undergo reduction at high temperature and low oxygen partial pressures, which introduces electronic defects and thus shorts the circuit [6]. The disadvantage of the reducibility can be avoided, for example, by coating the mixed conductive ceria material with a thin protective layer of purely ionic conductive zirconia, thereby blocking the electronic leak current.

Alkaline earth oxides, e.g. CaO, SrO, MgO, and BaO [7, 8], and rare earth oxides, e.g. Gd_2O_3 [9], La_2O_3 [10], and Y_2O_3 [11], have been successfully used as dopants for CeO_2. These dopants are extensively soluble in the ceria sublattice. Substitution of aliovalent cations of lower valence for Ce results in the formation of oxygen vacancies to compensate the charge balance in the sublattice. Thus, the solid solution becomes predominantly ionic conductive for oxygen vacancies over an extended temperature and oxygen pressure range.

Ceria-rare earth oxide systems as characterized by their large solubility limit and their electrical properties have been partially reported. Among the ceria electrolytes, samaria-doped ceria (SDC), $Sm_{0.2}Ce_{0.8}O_{1.9}$, was found to have the highest ionic conductivity [12, 13, 14]. However, the conductivity of the $(CeO_2)_{1-x}(SmO_{1.5})_x$ system has not yet been fully studied or explained definitely as a function of the additive content at the high temperature at which the solid-oxide fuel cell works. In the present work, the oxygen vacancy conductivity of the ceria-samaria system was investigated as a function of dopant concentration and temperature.

It has been found empirically that the temperature dependence of the conductivity can be expressed by an equation of the Arrhenius form:

$$\sigma T = A \exp\left(\frac{-E_a}{kT}\right) \tag{1}$$

where A is a constant, E_a is the activation energy, and k is the Boltzmann constant. When $\ln(\sigma T)$ is plotted against $1/T$, a straight line should be observed with the slope $(-E_a/k)$ and an intercept on the $\ln(\sigma T)$ axis of A. This is usually the case when the work is performed at low temperature. However, when the work is performed at high temperature, a curvature of the Arrhenius plot may be observed. Two straight-line portions of different slopes have been reported [14]. The portion at lower temperature has been explained by the interaction between mobile oxygen vacancies and immobile cations with dilute dopant concentration. Nevertheless, for higher dopant concentration, this may fail to explain the phenomenon of the curvature.

In this study, we attempt to explain the curvature phenomenon by a model of the nucleation center of the vacancy cluster, and also explain the critical temperature and the trapping energy variations with the dopant concentration.

Experimental

Sample preparation

The samples $(CeO_2)_{1-x}(SmO_{1.5})_x$ $(0.05 < x < 0.3)$ were prepared from reagent grade (99% purity, Aldrich) metal nitrates, $Sm(NO_3)_3{\cdot}6H_2O$ and $Ce(NO_3)_3{\cdot}6H_2O$. The appropriate proportions of samarium nitrate and cerium nitrate were dissolved in distilled water to make 0.1–0.2 M solutions. Hydrolysis of the metal salts to hydroxides was obtained by dropping into NH_4OH solution. To eliminate inhomogeneous gels, nitrate solutions were added dropwise to a 4N solution of NH_4OH and the solution was maintained at pH > 9. A distinct deeply purple color of precipitate gel was formed when the nitrate solution was dropped into the NH_4OH solution. The gel was easily isolated by vacuum filtration. The recovered gel was immersed in octanol and boiled on a hot plate. During boiling the gel shrunk substantially and the color changed from purple to black. The gel was dried at 130 °C in a tubular drier overnight to remove the solvent. After heating at 700 °C for 3 h, the powder with soft agglomerates was pressed and sintered, at 1300 °C for 5 h, into highly dense (95–98%) ceramic pellets.

X-ray analysis

The X-ray analysis technique was used to determine the crystal structure and phase. X-ray spectra were obtained over the 2θ range of 20–80° at a speed of 10°/min by a Phillips diffractometer (PW1710) with $Cu(K_\alpha)$ radiation. The diffractometer was operated at 40 kV and 40 mA. The results showed that, in the composition range 5–30 mol% $SmO_{1.5}$, no phase other than the cubic one with the fluorite structure could be identified.

Measurement of electrical conductivity

The electrical conductivity of a sintered sample was measured as a function of temperature by a conventional d.c. four-probes method (Van der Pauw method). The pellet was positioned in a resistance-heated furnace at predetermined distances using platinum lead wires. The pellet sample being measured was assumed to be of uniform thickness d with no holes within its circumference. Small contacts were placed on the circumference of the sample and designated as a, b, c, and d. The contact area was coated with platinum paste to eliminate contact resistance. Two values of resistance were measured:

1. $R_{ab,cd}$: ratio of potential difference developed between terminals cd to the current passing through the terminals ab.
2. $R_{bc,ad}$: ratio of potential difference developed between terminals bc to the current passing through the terminals ad.

The resistivity can be shown as:

$$R = (\pi d/\ln 2) \times \left(R_{ab,cd} + R_{bc,ad}\right)/2 \times fn\left[R_{ab,cd}/R_{bc,ad}\right] \tag{2}$$

where $fn[R_{ab,cd}/R_{bc,ad}]$ has been reported previously [15].

Results and discussion

In this work, it was assumed that the electronic contribution to the overall conductivity was negligible, i.e., $t_{ionic} = 1$. This assumption is reasonable, since all measurements were done in air at a temperature lower than 1000 °C and with dopant concentration less than 40 mol%. Although Ce^{4+} can be reduced to Ce^{3+} [6], this reduction could only occur in a reducing atmosphere and especially at higher temperature. A mixed Ce^{3+}/Ce^{4+} valence will introduce electronic conduction in addition to the oxygen vacancy conductivity. However, no evidence for the existence of electronic conductivity was observed in this study. Therefore, the electrical conductivity measured in this study is considered to be completely due to ionic conduction.

The composition dependence of the conductivity of the $(CeO_2)_{1-x}(SmO_{1.5})_x$ system is shown at different temperatures in Fig. 1. Basically, pure ceria oxide is a poor oxygen vacancy conductor ($\sigma_{600\,^\circ C} \approx 10^{-5}$ S/cm) [5]. The addition of $SmO_{1.5}$ enhanced the conductivity of the electrolyte system because of the formation of a large amount of oxygen vacancies, $V_{\ddot{o}}$, in the fluorite lattice, as expressed by the following reaction:

$$2SmO_{1.5} \xrightarrow{CeO_2} 2Sm'_{Ce} + O_O + V_{\ddot{O}} \tag{3}$$

where Sm'_{Ce} is a Sm^{3+} ion in a Ce^{4+} lattice site with negative charge.

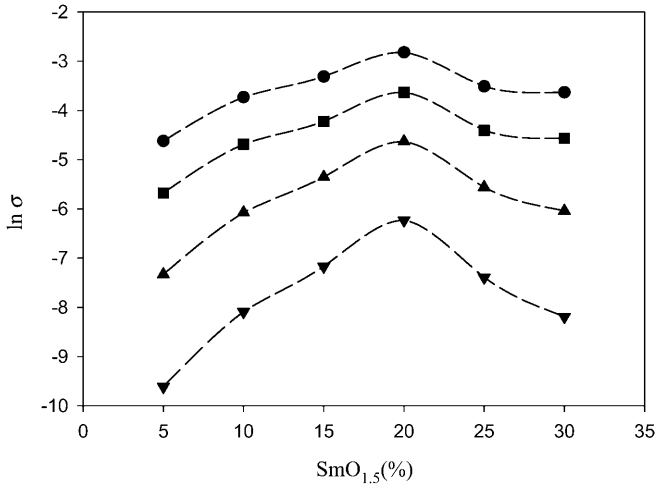

Fig. 1 Composition dependence of conductivities for $(CeO_2)_{1-x}(SmO_{1.5})_x$ at different temperatures: 500 °C (*down triangles*), 600 °C (*up triangles*), 700 °C (*squares*), 800 °C (*circles*)

The conductivity of $(CeO_2)_{1-x}(SmO_{1.5})_x$ increased and reached a maximum at $x=0.2$, which was 5.6×10^{-1} S/cm at 800 °C and close to the value of 4×10^{-1} S/cm as reported by a previous study [14]. Note that this is one order of magnitude higher than that of the stabilized zirconia at the same temperature. Also note that the oxygen vacancy conductivity of $(CeO_2)_{0.8}(SmO_{1.5})_{0.2}$ is two orders of magnitude higher than that of pure ceria in the range 500–800 °C. The decrease in conductivity when x is larger than 0.2 was gradual, as compared with that reported for doped zirconia [4]. The number of oxygen vacancies increased with increasing dopants within its solubility limit to maintain charge neutrality; however, the conductivity decreased even within the solubility limit. This implies a decrease in the mobility of vacancies at higher dopant concentration.

The increase of conductivity primarily results from the decrease in activation energy, as shown in Fig. 2. Our explanation is similar to that of Faber et al. [16] for $(CeO_2)_{1-x}(YO_{1.5})_x$. The decrease of activation energy results from attractive interactions between immobile dopant cations and mobile oxygen vacancies. When the amount of dopant increases, the oxygen vacancies interact with more dopant cations. The energy of an oxygen vacancy in a saddle-point between sites with interactions with dopant will be lower than that in a saddle-point between sites without any interactions. As observed, the minimum activation energy occurs with a dopant concentration of 20 mol% $SmO_{1.5}$. At higher dopant concentrations, deeper traps are formed owing to the dopant cations closely neighboring each other, and thus the activation energy increases.

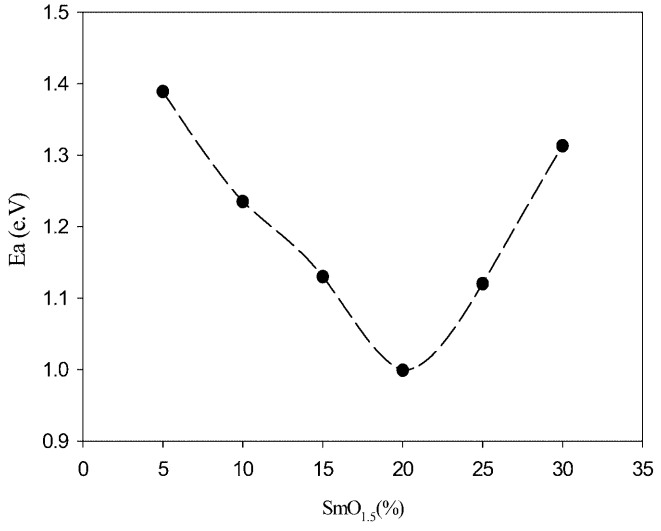

Fig. 2 Composition dependence of the activation energy

The Arrhenius plots of the conductivities in air are shown in Fig. 3. It is seen that a single straight line is not good enough to describe the reciprocal of the temperature dependence of the conductivities. For 20% SDC, one straight line in the Arrhenius plot for the full temperature scale was determined by fitting to a regression coefficient of 0.97. However, two straight lines with different slopes in the Arrhenius plot were determined by fitting to regression coefficients of 0.998 for both lines, as shown in Table 1. Therefore, a curvature should exist in the Arrhenius plot and it is necessary to further explore and find out the root cause for this curvature phenomenon.

In an oxygen vacancy electrolyte, the simplest model for the conduction is given by the random-walk theory [17]:

$$\sigma = n_c C q \mu = \left(\frac{A}{T}\right) \exp\left(\frac{-\Delta H_m}{kT}\right) \tag{4}$$

$$A = f\left(\frac{z}{6}\right)\left(\frac{Cq^2}{k}\right) n_c(1-n_c) l^2 v_o \exp\left(\frac{\Delta S_m}{k}\right) \tag{5}$$

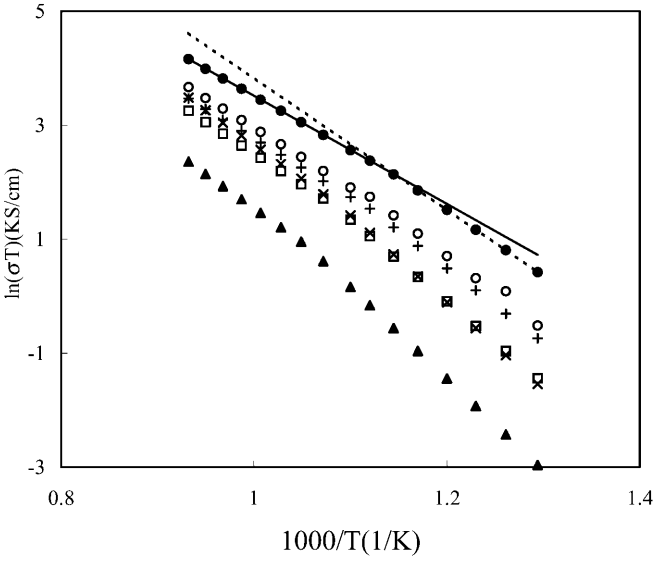

Fig. 3 Arrhenius plots of conductivities of $(CeO_2)_{1-x}(SmO_{1.5})_x$ for $x=0.05$ (*up triangles*); $x=0.1$ (*squares*); $x=0.15$ (*open circles*); $x=0.2$ (*filled circles*); $x=0.25$ (*plus signs*); $x=0.3$ (*crosses*)

Table 1 Regression coefficient for fitting one straight line (Y) or two straight lines (Y1 and Y2)

$SmO_{1.5}$	5%	10%	15%	20%	25%	30%
R^2(Y)	0.978	0.979	0.981	0.970	0.977	0.973
R^2(Y1)	0.996	0.997	0.996	0.998	0.993	0.999
R^2(Y2)	0.998	0.998	0.999	0.998	0.998	0.994

where the oxygen vacancy mobility $\mu = \frac{qD}{kT}$ is given by the Einstein equation for diffusive motion of a carrier of charge q; the diffusion coefficient $D = D_0 \exp\left(\frac{-\Delta G_m}{kT}\right)$ contains the motional free energy $\Delta G_m = \Delta H_m - T\Delta S_m$ for a jump to an occupied, equivalent near-neighbor site. In Eq. 5, l is the distance to the z nearest-neighbor equivalent sites having a probability of being occupied, C is the density of equivalent sites on which n_cC mobile vacancies move, n_c is the fraction of these sites that are empty, v_o is the optical-mode attempt frequency for an jump, and f is the geometrical factor of order unity that depends on the jump path. For a fluorite unit cell with $l = a/2$, $z = 6$, $f \approx 1$, $q = 2e$, and $C = 4a^{-3}$, Eq. 5 is reduced to

$$A = \left(\frac{4e^2}{ka}\right) n_c(1 - n_c) v_o \exp\left(\frac{\Delta S_m}{k}\right) \tag{6}$$

From Eq. 4, the plot of $\ln(\sigma T)$ versus $1/T$ should give a straight line of slope $-\Delta H_m/k$. However, as shown in Fig. 3, a distinct curvature can be observed in the Arrhenius plot for oxygen vacancy conduction. In these systems, the dopant cations may not only act just as traps for isolated vacancies, but also as nuclei for the formation of ordered-vacancy clusters. The simplest model for such a system of nucleation would consist of a cation as a nucleation center with negative charge having a critical temperature T_c: below T_c, the oxygen vacancies with positive charge are progressively trapped in the clusters with decreasing temperature; above T_c, the vacancies are dissolved into the matrix of the normal sites. A treatment of this model is similar to that for dissolution of a solid solution into a liquid solution. If the chemical potentials of the solid and the liquid solutions with random distribution of vacancies are μ(sol) and μ(liq), respectively, and assuming the system is an ideal solution, then:

$$\mu(\text{liq}) = \mu^\circ(\text{liq}) + kT \ln\left(\frac{n_c^*}{n_c^*}\right) \tag{7}$$

and:

$$\mu(\text{sol}) = \mu^\circ(\text{sol}) + kT \ln\left(\frac{n_c}{n_c^*}\right) \tag{8}$$

where n_c* is the total fraction of oxygen vacancies that exist in the absence of nucleation, and n_c/n_c* is the fraction of oxygen vacancies that are dissolved in random positions in the oxygen vacancy sublattice. At equilibrium the chemical potential of each component is the same in the coexisting phase. Hence, the chemical potential for each vacancy component is the same in the solid as in the liquid, i.e.:

$$\Delta H_t - T_c \Delta S_t = \Delta G_t(T_c) = 0 \rightarrow \Delta S_t = \frac{\Delta H_t}{T_c} \tag{9}$$

where ΔH_t is the trapping energy between vacancies and cations. Because the standard states of the disordered μ°(liq) and ordered μ°(sol) phases are the same, it follows that, at temperature $T < T_c$, the Gibbs free energy for trapping liquid vacancies into clusters, $\Delta G_t(T) = \mu(\text{sol}) - \mu(\text{liq})$, is equal to:

$$\Delta H_t - T\Delta S_t = kT \ln\left(\frac{n_c^*}{n_c}\right) \tag{10}$$

For small n_c*, substitution of Eq. 9 into Eq. 10 leads to:

$$\ln\left(\frac{n_c}{n_c^*}\right) = \left(-\frac{\Delta H_t}{kT}\right)\left(1 - \frac{T}{T_c}\right) \tag{11}$$

provided ΔH_t and ΔS_t for the condensate are independent of temperature. Combining Eq. 11 with Eqs. 4 and 6 gives:

$$\ln(\sigma T) = \ln A - \left(\frac{\Delta H_m}{kT}\right) \tag{12}$$

$$A = A' \exp\left[\left(\frac{-\Delta H_t}{kT}\right)\left(1 - \frac{T}{T_c}\right)\right] \tag{13}$$

$$A' = \left(\frac{4e^2}{ka}\right) v_o n_c^* \exp\left(\frac{\Delta S_m}{k}\right) \tag{14}$$

Substituting A in Eq. 13 into Eq. 12 gives:

$$\ln(\sigma T) = \ln\left[A' \exp\left(\frac{\Delta H_t}{kT_c}\right)\right] - \left(\frac{\Delta H_m + \Delta H_t}{kT}\right) \tag{15}$$

for $T < T_c$. For $T > T_c$:

$$\ln(\sigma T) = \ln(A') - \left(\frac{\Delta H_m}{kT}\right) \tag{16}$$

Similar expressions have been derived by Huang et al. [18, 19]. According to Eqs. 15 and 16, the Arrhenius plot would give two straight lines, which intersect at T_c, with activation energies $E_1 = \Delta H_m$ and $E_2 = \Delta H_m + \Delta H_t$, and with preexponential terms $A_1 = A$' and $A_2 = A$'$\exp(\Delta H_t/kT_c)$, respectively, as shown in Fig. 4 for the 20% SDC case. The preexponential factor, the activation energy,

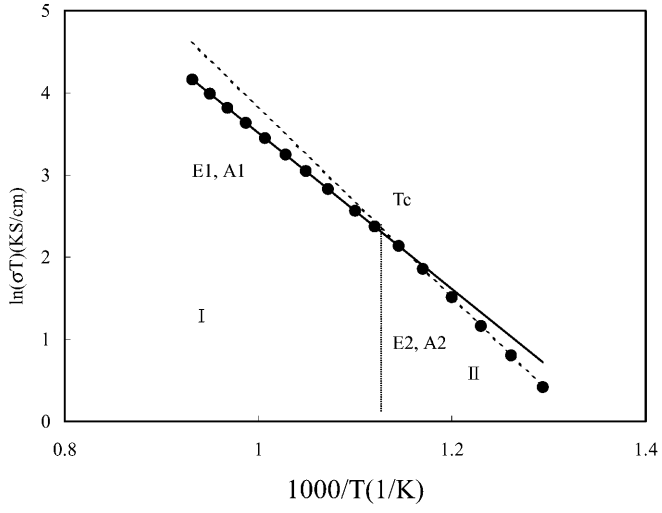

Fig. 4 Illustration of the curvature separated by T_c into two regions I and II

and the critical temperature are listed in Table 2. The motional free energy obtained from this model is 0.82 eV for 20% SDC, which is similar to the value of 0.78 eV for the activation energy reported elsewhere [12].

From the above model of the nucleation center of the vacancy cluster, the trapping energy can be obtained. The composition dependence of the trapping energy is shown in Fig. 5. From this figure, a plot of trapping energy versus dopant concentration shows a minimum at 20% $SmO_{1.5}$. This tendency is clearly consistent with that of the activation energy as shown in Fig. 2. Thus, the extra energy, i.e., the trapping energy, needed for an oxygen vacancy to move from a regular site to the saddle-point decreases with the increase of the dopant cations and reaches a minimum at 20% $SmO_{1.5}$. However, at higher dopant concentrations the dopant ions become so close to each other as to form deeper traps, which increase the energy needed to bring the oxygen vacancy from a regular site to the saddle point.

The composition dependence of the critical temperature is shown in Fig. 6. It is not surprising that a minimum also occurs at 20% $SmO_{1.5}$, which agrees with the model of the nucleation center of the vacancy cluster. The minimum implies that the energy needed to break the interaction between the cation and the oxygen vacancy decreases with the decrease of the interaction between the cation and the oxygen vacancy.

It is thus concluded that the composition dependences of the critical temperature and the trapping energy are both consistent with that of the activation energy and show a minimum with a doping of 20 mol% $SmO_{1.5}$. It may also be concluded that the model of the nucleation center of the vacancy cluster can explain the variation of the activation energy, the critical temperature, and the trapping energy with the dopant concentration.

Table 2 Electrical properties of $(CeO_2)_{1-x}(SmO_{1.5})_x$

X	ln A_1	E_1 (eV)	ln A_2	E_2 (eV)	T_c (°C)
0.05	13.59	1.04	17.87	1.39	673
0.1	13.45	0.95	17.08	1.24	652
0.15	13.11	0.90	16.20	1.13	625
0.2	13.00	0.82	15.42	1.00	591
0.25	13.43	0.90	16.28	1.12	620
0.3	14.75	1.04	18.16	1.31	645

Conclusions

For the samaria-doped ceria electrolyte, it has been shown that a maximum in conductivity versus dopant concentration corresponds to a minimum in activation energy.

It is found that the conductivity is completely due to oxygen vacancy conduction. The conductivity increases with increasing samaria doping and reaches a maximum for $(CeO_2)_{0.8}(SmO_{1.5})_{0.2}$, which has a conductivity of 5.6×10^{-1} S/cm at 800 °C.

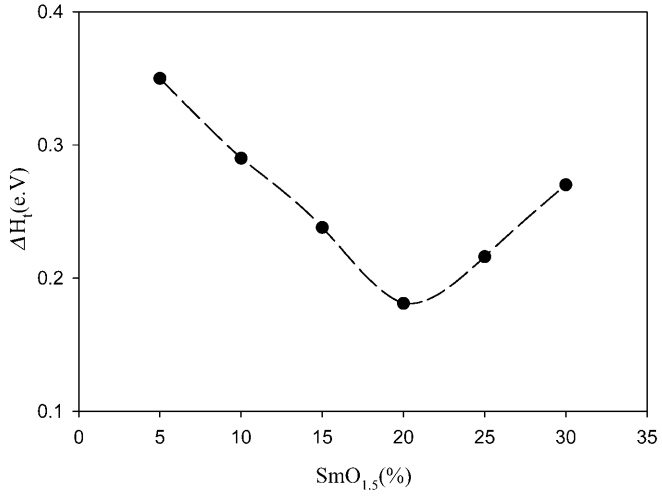

Fig. 5 Composition dependence of the trapping energy

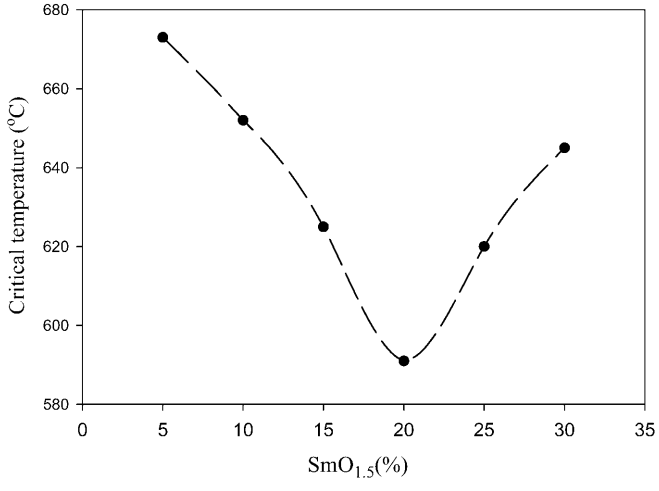

Fig. 6 Composition dependence of the critical temperature

It is also found that the conductivity does not obey the Arrhenius relationship. A marked curvature has been found at $T = T_c$, the critical temperature. To explain this phenomenon, a model has been proposed that, below T_c, the oxygen vacancies condense into clusters of ordered vacancies; above T_c, all vacancies appear to be mobile.

In addition, it is concluded that the composition dependences of the critical temperature and the trapping energy are both consistent with the tendency of the activation energy and show a minimum at the dopant concentration of 20 mol% $SmO_{1.5}$.

References

1. Riley B (1990) J Power Sources 29:223
2. Eguchi K, Setoguchi T, Inoue T, Arai H (1992) Solid State Ionics 52:165
3. Subbarao E, Maiti HS (1984) Solid State Ionics 11:317
4. Steele BCH (1994) J Power Sources 49:1
5. Yahiro H, Baba Y, Eguchi K, Arai H (1988) J Electrochem Soc 135:2077
6. Tuller HL (1992) Solid State Ionics 52:165
7. Yahiro H, Ohuchi T, Eguchi K, Arai H (1988) J Mater Sci 23:1036
8. Arai H, Kunisaki T, Shimizu Y, Seiyama (1986) Solid State Ionics 20:241
9. Hatchwell C, Sammes NM, Brown IWM (1999) Solid State Ionics 126:201
10. Dikmen S, Shuk P, Greenblatt M (1999) Solid State Ionics 126:89
11. Wang DY, Park DS, Griffith J, Nowick AS (1981) Solid State Ionics 2:95
12. Yahiro H, Egushi Y, Arai H (1988) J Appl Electrochem 18:527
13. Egushi Y, Setoguchi T, Inoue T, Arai H (1992) Solid State Ionics 52:165
14. Balazs GB, Glass RS (1995) Solid State Ionics 76: 155
15. Blumental RN, Seitz MA (1974) Electrical conductivity in ceramics and glass. Dekker, New York
16. Faber J, Geoffroy A, Roux A, Sylvestre A, Abelard P (1989) Appl Phys A 49:225
17. Bruce PG (1995) Solid state electrochemistry. Cambridge University Press, Cambridge
18. Huang KQ, Feng M, Goodenough JB (1998) J Am Ceram Soc 81:357
19. Huang KQ, Tichy RS, Goodenough JB (1998) J Am Ceram Soc 81:2565